Lab Notes

Figure 1. This 0.59 ct near-colorless octagonal step-cut armenite measuring 6.01 × 4.07 × 3.33 mm marks the first time this mineral has been submitted to a GIA laboratory. Photo by Diego Sanchez.

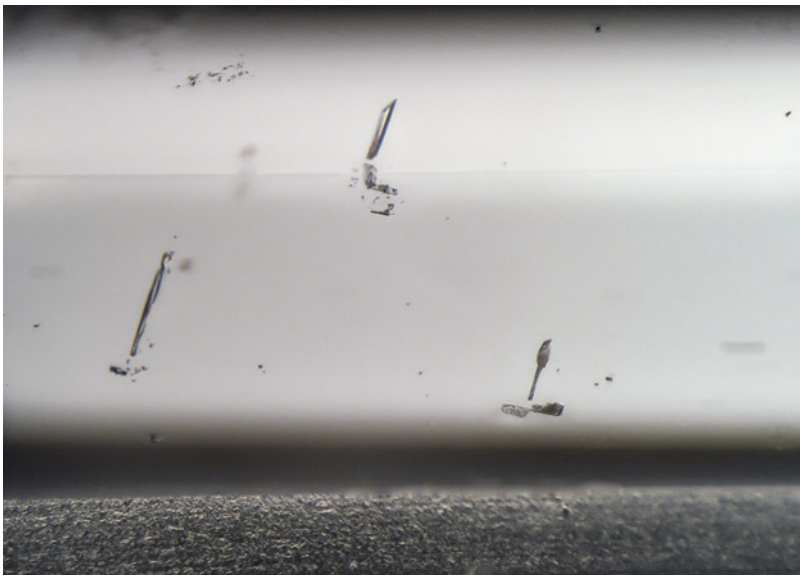

Figure 2. Negative crystal inclusions were observed in the submitted armenite. Photomicrograph by Britni LeCroy; field of view 2.77 mm.

Rare Faceted ARMENITE

A 0.59 ct near-colorless octagonal step-cut stone was recently submitted to the Carlsbad laboratory (figure 1). Standard gemological testing measured a refractive index of 1.550–1.555 (birefringence of 0.005), a biaxial optic figure, and a hydrostatic specific gravity of 2.77. Microscopic examination revealed negative crystals (figure 2), colorless particles, and a small fingerprint breaking the pavilion surface. These properties were consistent with those reported for armenite. The submitted stone was then compared to a near-colorless armenite reference specimen belonging to the GIA Museum, which showed a similar microscopic appearance along with internal stress fractures. Raman and infrared spectra collected on both stones were a near-perfect match, further supporting the armenite identity of the stone.

Armenite is a rare orthorhombic silicate with a formula of $BaCa_2Al_6Si_9O_{30}{\cdot}2(H_2O)$. Originally identified in Norway in 1939, it has since been found in Canada (Quebec), Australia (New South Wales), Scotland, the Czech Republic, Switzerland, the United States (Washington), and Italy (Sardinia). It usually forms as veins within host rocks, including metasomatic basic to intermediate igneous rocks, mineralized skarn and hornfels, and gneisses. The data gathered from this first-time submission of armenite will assist in future identifications.

Britni LeCroy

Editors' note: All items were written by staff members of GIA laboratories.

Gems & Gemology, Vol. 61, No. 4, pp. 392–399.

Figure 3. A 100.15 ct faceted cuprite, measuring 29.37 × 22.29 × 14.09 mm, the largest ever submitted to GIA. Photo by Diego Sanchez.

100 ct CUPRITE with Malachite Inclusions

The Carlsbad laboratory recently examined a 100.15 ct transparent dark red gem submitted for an identification report (figure 3). An over-the-limit refractive index reading and submetallic luster were observed. Raman and infrared spectra were collected on the stone and concluded its identity as cuprite. This is the largest cuprite ever submitted to GIA. While its size alone makes the stone noteworthy, it also possessed photogenic malachite inclusions identified with Raman spectroscopy. Most were in the form of small, concentrically banded green aggregates breaking the surface of the pavilion (figure 4). But the most interesting inclusion was a cluster of dark green transparent malachite crystals breaking the crown (figure 5). Transparent crystals are uncommon for this mineral.

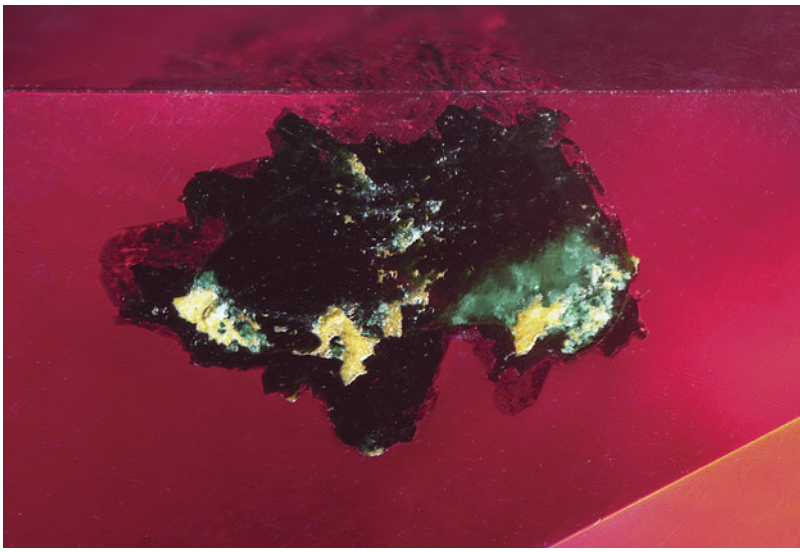

Figure 5. A cluster of dark green transparent malachite crystals breaks the crown of the cuprite. Photomicrograph by Britni LeCroy; field of view 2.81 mm.

Cuprite is an oxide mineral with the simple chemical formula of Cu_2O. It is a secondary mineral that forms in the oxidized zone of copper sulfide deposits. Large, gem-quality specimens are exceptionally rare and are most often sourced from a single deposit in Namibia. Cuprite is often found with malachite, a copper carbonate hydroxide mineral, along with azurite, chalcocite, and limonite. Gem-quality cuprite is mainly considered a collector's stone. While the mineral has an attractive deep red hue and submetallic luster, its Mohs hardness is 3.5–4, making it generally too soft for use in jewelry.

Britni LeCroy

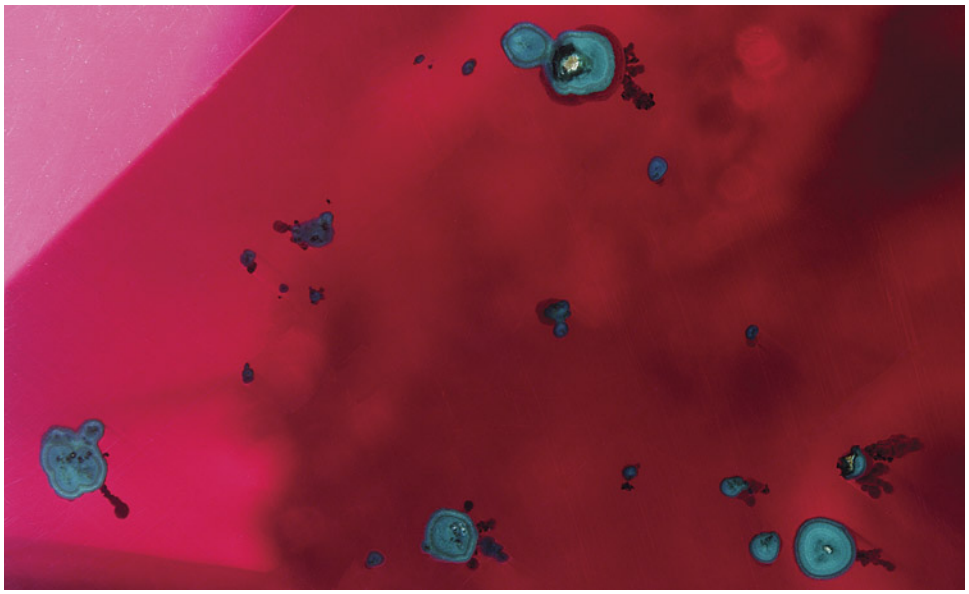

Figure 4. Banded aggregate malachite inclusions were observed breaking the pavilion of the cuprite. Photomicrograph by Britni LeCroy; field of view 4.74 mm.

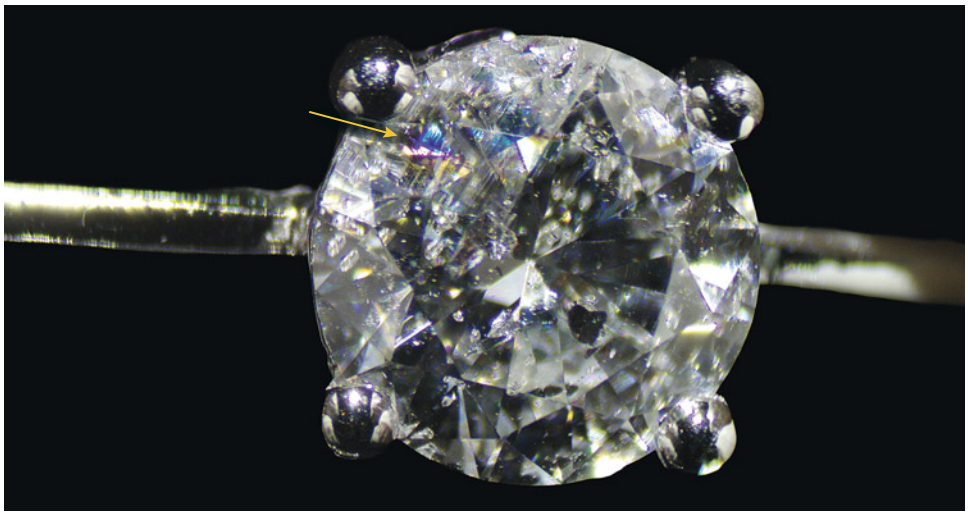

Figure 6. A round brilliant-cut diamond set in the necklace exhibits the flash effect (indicated by arrow) when tilted, a characteristic of fracture filling caused by the presence of a filler within a surface-reaching fracture. Photo by Gaurav Bera.

Fracture-Filled DIAMONDS Detected in Mounted Jewelry

Since the introduction of GIA's Jewelry Analysis Service at the India International Jewellery Show (IIJS) Premiere in August 2025, the Mumbai laboratory has received several intriguing submissions. Among them was a set of mounted items: a pair of earrings and a necklace. The necklace featured 14 round brilliants with a stated weight of 15.27 carats total. The earrings were set with a combination of pear-, oval-, and marquise-shaped stones with a stated weight of 10.84 carats total.

In both the necklace and earrings, the prongs limited access to the pavilion areas and restricted a full view of clarity features. Spectroscopic analysis using the GIA iD100 confirmed that all mounted stones were diamonds and ruled out a laboratory-grown origin. During clarity assessment, bright rainbow-like reflections were observed in two round diamonds from the necklace and in one marquise-shaped diamond from an earring. These features were visible face-up under 10× magnification. At 40× magnification under darkfield and fiber-optic illumination, the phenomenon was identified as the flash effect (figure 6), a visual characteristic typically associated with fracture-filled diamonds (Spring 2018 Lab Notes, pp. 56–57). Flash effects can be challenging to detect, as surface-reaching fractures may show iridescence. Viewing angle is critical for accurate identification; iridescence is typically visible when viewed nearly perpendicular to the fracture plane, whereas the flash effect appears most clearly when viewed parallel to the plane. In addition to the flash effect, a cloudy, milky area was observed across crown facets of the marquise-shaped diamond, further supporting the presence of a filler material within the fracture (figure 7).

Fracture filling is a clarity enhancement treatment used to improve the visual appearance of diamonds by filling surface-reaching fractures with a glass-like substance. The filler material (typically a lead-containing glass) has a refractive index close to that of diamond, reducing the visibility of the fractures and thus giving an appearance of improved clarity (S.F. McClure and C.P. Smith, "Gemstone enhancement and detection in the 1990s," Winter 2000 *G&G*, pp. 336–359). Unlike some clarity treatments that are stable and long-lasting, fracture filling is not permanent; the filler may degrade or become discolored over time, particularly when exposed to ultraviolet light, heat, ultrasonic cleaning, or certain chemicals. The presence of such unstable treatments significantly impacts a diamond's value, durability, and required care. Because of the unstable nature of the filler, GIA does not issue grading reports for diamonds that have undergone fracture filling. Therefore, thorough testing, especially of mounted stones, remains essential for accurate grading and identification. Full disclosure of such treatments is crucial to uphold consumer confidence and ensure market transparency.

Sumit Vardawat, Ashok Prajapati, and Roxane Bhot Jain

Figure 7. A marquise-shaped diamond set in one of the earrings displays a cloudy appearance (indicated by arrow) caused by the presence of filler material within surface-reaching fractures. Photo by Gaurav Bera.

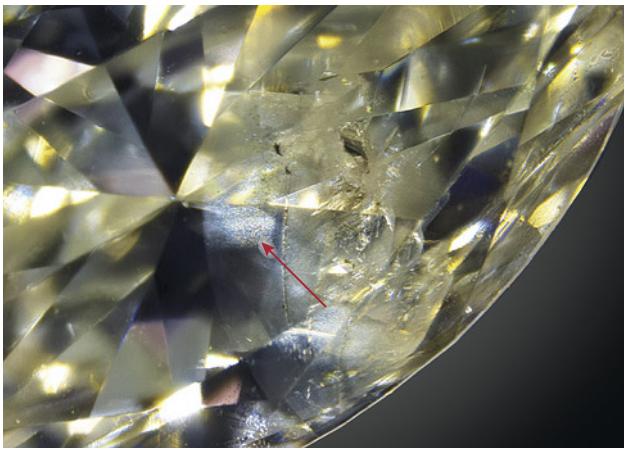

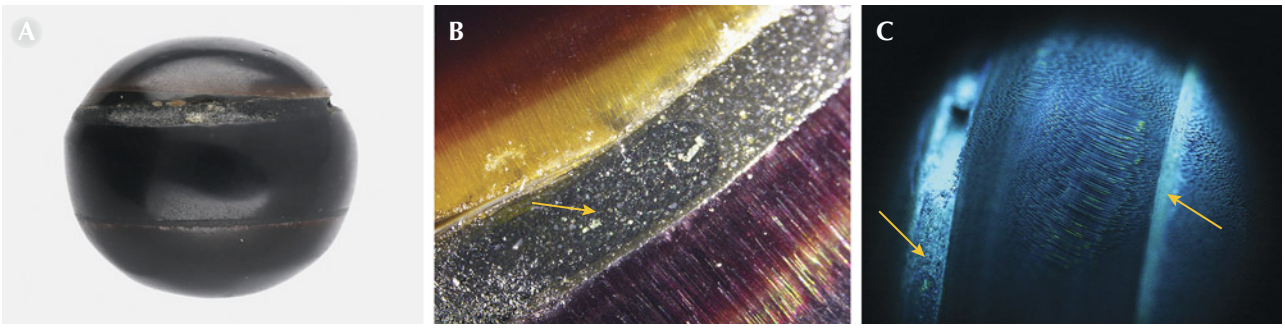

Figure 8. A: An assembled black non-nacreous imitation pearl weighing 10.56 ct and measuring 12.23 × 11.87 × 10.78 mm. B: Bonding agent (indicated by arrow) between the two shell fragments with the polishing lines exhibiting an optical chatoyancy-like effect where colors of pink, yellow, and green were observed. C: Strong bluish green fluorescence observed under the DiamondView showing banding of an unidentified bonding agent (arrows) along with the calcitic columnar structure. Photos by Gaurav Bera (A) and Keaton Talker (B and C); field of view 4.30 mm (B).

Assembled Black IMITATION PEARL

GIA's Mumbai laboratory recently examined an undrilled black near-round bead, weighing 10.56 ct and measuring 12.23 × 11.87 × 10.78 mm, submitted for identification (figure 8A). Initial examination of the specimen indicated that it was an assembled imitation pearl made from shell fragments.

Visually, the specimen consisted of three distinct sections fused together using a dark-colored bonding agent. Under high magnification, some areas revealed columnar structures similar to those observed in non-nacreous pen pearls from the Pinnidae family. Fine lines from working and polishing the specimen were visible across the surface, likely created during the shaping process. Interestingly, under fiber-optic illumination, a chatoyancy-like phenomenon was created by the fine acicular structure of calcite crystals of the shell (figure 8B). When examined using the deep-UV wavelength (<230 nm) of the DiamondView, the three fragments exhibited prominent bands with a bluish reaction and fine cellular hexagonal calcitic columnar features typical of a pen shell (figure 8C; Spring 2017 *G&G* Micro-World, pp. 105–106). The bonding agent displayed a stronger bluish green reaction.

The specimen showed an inert reaction under X-ray fluorescence. Energy-dispersive X-ray fluorescence analysis conducted on the three fragments revealed no traces of manganese but strontium levels of 639, 819, and 904 ppm, respectively, indicating that they were of saltwater origin. Real-time X-ray microradiography (RTX) displayed a distinct banding pattern wherein demarcations were visible between the shell fragments and the bonding agent (figure 9A). The shell fragments exhibited a tight structure. X-ray computed microtomography (μ-CT) imaging showed a more defined banding structure and gas bubbles trapped within the bonding agent (figure 9, B and C). All these characteristics were similar to those previously observed in imitation pearls made of pen shell (Fall 2019 Gem News International, pp. 445–446).

Collectively, the analytical data and observations indicated that the three fragments originated from the same kind of shell, possibly pen shell, and were bonded to create an imitation resembling a whole non-nacreous pen pearl.

Keaton Talker, Roxane Bhot Jain, and Abeer Al-Alawi

Figure 9. A: RTX image showing the three shell fragments fused by a bonding agent (indicated by arrows). B: μ-CT imaging displaying a very tight structure with internal banding (arrow). C: μ-CT imaging showing trapped gas bubbles (white arrows) within the bonding agent (yellow arrow).

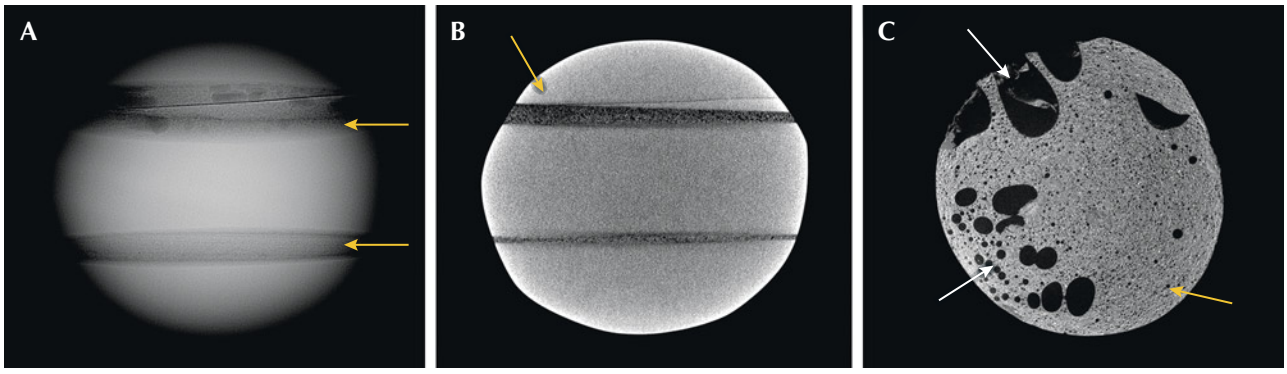

Figure 10. An orangy red translucent friedelite weighing 27.50 ct. Photo by Diego Sanchez.

A Rare FRIEDELITE

The Carlsbad laboratory recently received an orangy red translucent stone weighing 27.50 ct and measuring approximately 22.46 × 22.11 × 7.42 mm (figure 10). Standard gemological testing revealed a spot refractive index of 1.63 and an absorption band between ~535 and 595 nm with a cutoff of ~480 nm using a handheld spectroscope. The stone contained a long but shallow eye-visible fracture that had been stained black by an unknown substance. A cryptocrystalline aggregate structure was observed under the microscope, with the stone remaining light when rotated in the polariscope. The center of the stone displayed a uniform orangy red color. Small white blebs of carbonate mineralization above a veinlet of white and pink carbonate minerals were found along the perimeter of the stone (figure 11). These observations, along with Raman spectroscopy, were consistent with the rare mineral friedelite ($Mn_8^{2+}Si_6O_{15}(OH,Cl)_{10}$).

Figure 11. Small white blebs of carbonate mineralization above a veinlet of white and pink carbonate minerals in a rare orangy red friedelite. Photomicrograph by Michaela Damba; field of view 6.34 mm.

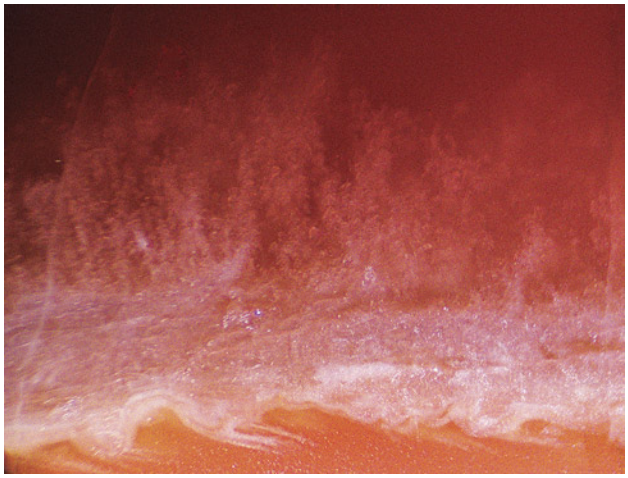

Friedelite was first discovered in 1876 in the manganese mine at Adervielle, in the Vallée du Luron of the Hautes Pyrenees, France, and named after French chemist and mineralogist Charles Friedel. Since its discovery, friedelite occasionally has been found worldwide in other manganese silicate deposits (H.S. Pienaar, "Gem-quality friedelite from the Kalahari manganese field near Kuruman, South Africa," Winter 1982 *G&G*, pp. 221–224). This is the second friedelite GIA has examined to date.

Michaela Damba

Cat's-Eye Boulder OPAL

The Carlsbad laboratory recently encountered a 4.80 ct cushion-shaped double cabochon, measuring 11.65 × 9.87 × 4.71 mm, submitted for identification. The cabochon's specific gravity measured 2.68 with a spot refractive index reading of 1.44, consistent with boulder opal. The stone was characterized as a translucent precious cat's-eye boulder opal with an opaque ironstone matrix base. Its dark gray bodycolor was influenced by a cloudy layer of minute inclusions at the precious opal–ironstone matrix boundary. The uneven boundary and color pattern indicated the stone's natural creation, showing no evidence of assembly or treatment and no fluorescence when exposed to ultraviolet light. The chatoyant play-of-color band stayed dominantly green as a light source moved across the stone, with flashes of blue play-of-color mingling with the green (figure 12). Chatoyant bands in precious cat's-eye opal are not always one color; while more centered and well-defined in comparison to this boulder opal, a solid green chatoyant band has been similarly observed, displaying an "opening" of the eye under two light sources (Summer 2003 Lab Notes, p. 148).

Figure 12. This composite image of a 4.80 ct precious cat's-eye boulder opal shows the progression of the cat's-eye as a light source moves across the stone. Photos by Annie Haynes.

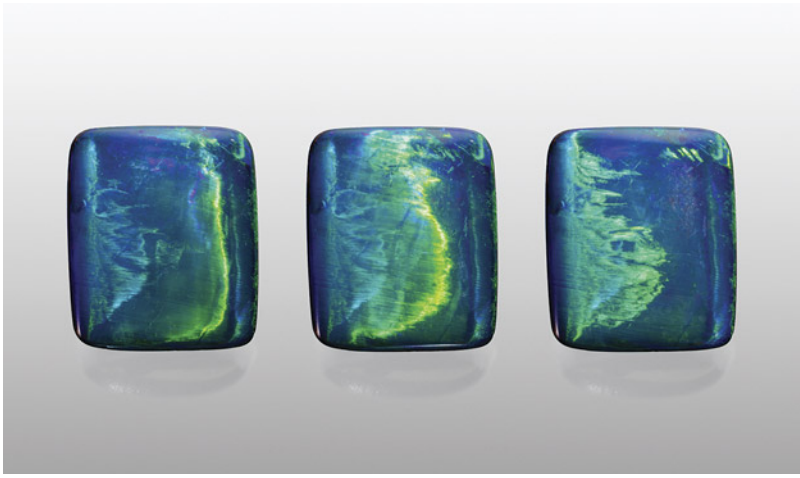

Precious opal is often associated with unique mosaic patterns attributed to its play-of-color. This material can also display other phenomena such as asterism (Summer 2014 Lab Notes, pp. 152–153) or chatoyancy. Both phenomena are quite uncommon due to opal's lack of a definite repeating crystal structure (J.V. Sanders, "The structure of star opals," *Acta Crystallographica*, Vol. A32, 1976, pp. 334–338). Most cat's-eye opals on the market today lack play-of-color; these are referred to as common opals and tend to have a brownish yellow bodycolor. Chatoyancy in common opal is caused by light reflecting off numerous parallel fibrous inclusions, as it is in most other cat's-eye gemstones. Common cat's-eye opal can originate from countries such as Tanzania and Brazil.

GIA laboratories occasionally examine rare precious cat's-eye opals with misalignments in their structure generating linearly arranged play-of-color patches. Precious cat's-eye opal has been sourced from various countries including the United States and Mexico (Winter 1990 Gem News, p. 304), with the sharpness of the eyes and the spectral colors observed varying greatly. Chatoyancy in precious opal can be affected by the cutting quality and orientation.

This cat's-eye boulder opal was reportedly sourced from the Opalton mining area, a locality in Queensland, Australia. Precious opal in boulder rough is rarely visible on the exterior of ironstone concretions. A periphery saw blade impregnated with industrial diamond is used to carefully slice at the edges of the concretion, exposing the opal. Slow grinding with the wheel when fashioning the stone gives definition to the cat's-eye, or "rolling flash" play-of-color pattern.

As the cat's-eye dissipated toward one side of the stone, a broad stroke of bluish green play-of-color resembling an aurora or bioluminescent ocean wave during an algae bloom took form. This unique type of boulder opal is a visually impressive and rare example of precious cat's-eye opal viewed from any face-up angle.

Jeffrey Hernandez

Figure 13. An 8.98 ct white semi-baroque cultured pearl measuring 11.31 × 10.75 × 10.30 mm exhibiting dents and wrinkles on its surface. Photo by Hemal Trivedi.

PEARLS

An Unconventional Bead Cultured Saltwater Pearl

GIA's Mumbai laboratory recently received an undrilled white semi-baroque saltwater nacreous pearl for identification, weighing 8.98 ct and measuring 11.31 × 10.75 × 10.30 mm (figure 13). Externally, the pearl exhibited dents and wrinkles on its surface, similar to those observed in cultured pearls.

Real-time X-ray microradiography (RTX) revealed a tight structure with uniform opacity throughout the pearl and the absence of growth features typical of natural or cultured origin in pearls of this size (figure 14A). The internal

Figure 14. RTX (A) and µ-CT (B) imaging showing the subtle variation in radiopacity between the bead nucleus and the nacre (indicated by arrow). C. µ-CT scan of a bead cultured pearl for comparison showing the demarcation of the bead nucleus with a small organic gap.

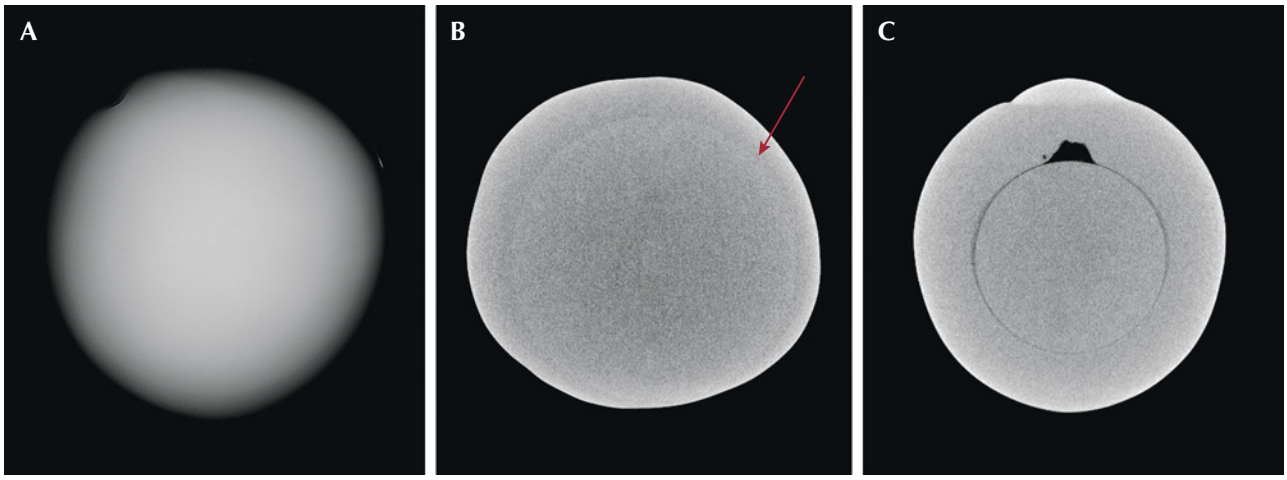

structure was challenging to interpret, requiring further analysis using X-ray computed microtomography (μ-CT) imaging, which also revealed a tight structure. However, a fine round demarcation of a possible bead nucleus was present, exhibiting a subtle variation in its radiopacity with an outer nacre area (figure 14B). This evidence indicated that the pearl was likely bead cultured, though it appeared atypical.

Typically, bead cultured pearls are easily identifiable as they show a characteristic distinct dark gray demarcation of the round bead nucleus used during the cultivation process (figure 14C), and sometimes are accompanied by small organic gaps. The examined pearl exhibited a more blended and uniform opacity throughout, with the bead nucleus appearing more radiopaque than traditional freshwater shell nuclei. The pearl displayed an inert reaction when subjected to X-ray fluorescence (XRF), indicating its saltwater origin. Moreover, this reaction suggests that the bead is of a non-standard material, as typical white saltwater bead cultured pearls with this nacre thickness (again, see figure 14B) usually exhibit weak yellowish green fluorescence under XRF due to trace amounts of manganese from the freshwater shell material of the bead. These observations suggest the potential use of an unconventional bead nucleus for culturing, such as a saltwater shell bead or other organic material (L.E. Cartier and M.S. Krzemnicki, "New developments in cultured pearl production: Use of organic and baroque shell nuclei," *Australian Gemmologist*, Vol. 25, No. 1, 2013, pp. 6–13).

Identifying the material used as the bead nucleus in this pearl remains inconclusive due to the lack of fluorescence and shell banding, coupled with the subtle variations in the radiopacity of the bead nucleus. Significant advancements in techniques and materials used for culturing pearls have resulted in an increased number of challenging pearls submitted for identification to laboratories. In a few cases similar to the pearl examined here, results based entirely on RTX imaging can lead to misidentification. The use of μ-CT imaging has proven to be a pivotal tool in the identification of such challenging pearls (M.S. Krzemnicki et al., "X-ray computed microtomography: Distinguishing natural pearls from beaded and non-beaded cultured pearls," Summer 2010 *G&G*, pp. 128–134).

Pfokreni Nipuni, Abeer Al-Alawi, and Chunhui Zhou

Filled Natural Hollow Heart-Shaped Pearls

Recently, the Mumbai laboratory received a parcel of loose white to light cream baroque pearls identified as filled natural hollow saltwater pearls after visual and chemical examination. Four of these pearls exhibited notable heart-like shapes and an unusual red X-ray fluorescence (figure 15).

The four pearls ranged from 22.47 × 22.00 × 15.73 mm to 35.46 × 27.27 × 24.22 mm in size and weighed 34.30, 52.75, 75.86, and 98.53 ct. They appeared worn and fragile, and their heft slightly exceeded the typical weight for pearls of similar size (Winter 2022 Lab Notes, pp. 480–481). Their surfaces were characterized by significant cracks, grooves, and plugged areas. When viewed under higher magnification, all four pearls revealed areas that were sealed with a piece of shell, bonded together using a yellowish brown resinous adhesive (figure 16A). This adhesive was visible within the cracks and fissures and contained trapped air bubbles (figure 16, B and C). While some surface areas exhibited an overlapping nacre terrace structure, there was also evidence of working observed near the plugged areas.

Real-time X-ray microradiography (RTX) and X-ray computed microtomography (μ-CT) analyses revealed the presence of large cavities filled with foreign materials, with a radiopacity similar to the pearls' nacre. Rectangular and tabular fragments of different sizes used as fillers were visible in the μ-CT images, as well as pieces of cut shell to seal the pearls' openings (figure 17). The smooth outline of these large cavities blended with the external shape of the pearls. In addition, the growth arc pattern of the surrounding nacre was an indicator of their natural formation. GIA has previously encountered similar pearls (Summer 2019 Lab Notes, pp. 251–254).

Energy dispersive X-ray fluorescence spectroscopy showed manganese levels below detection limits and strontium levels ranging from 790 to 1297 ppm, indicating a saltwater origin. When viewed under X-ray fluorescence, all four pearls showed red emission of varying intensity. Although most saltwater pearls are inert, this unusual red

Figure 15. Top: Four heart-shaped filled natural hollow pearls weighing 34.30, 52.75, 75.86, and 98.53 ct (from left to right). Bottom: The pearls exhibit red X-ray fluorescence of varying degrees. Photos by Gaurav Bera and Eram Shaikh.

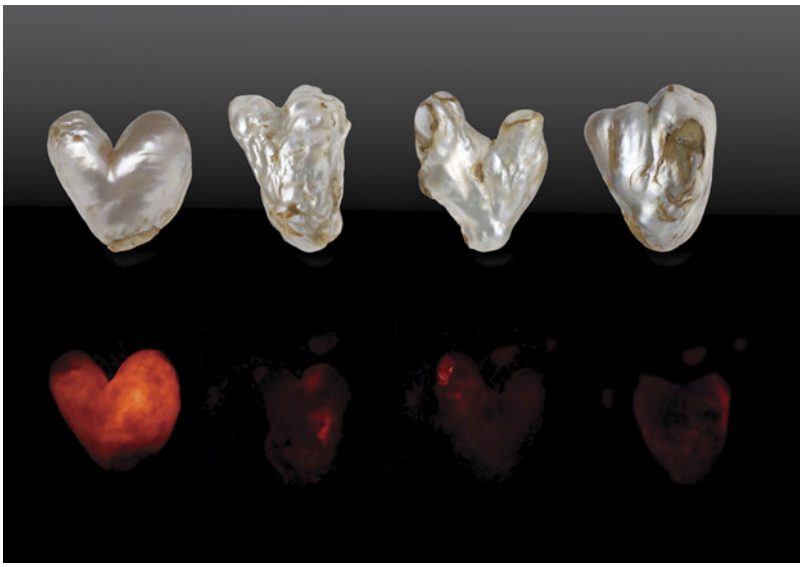

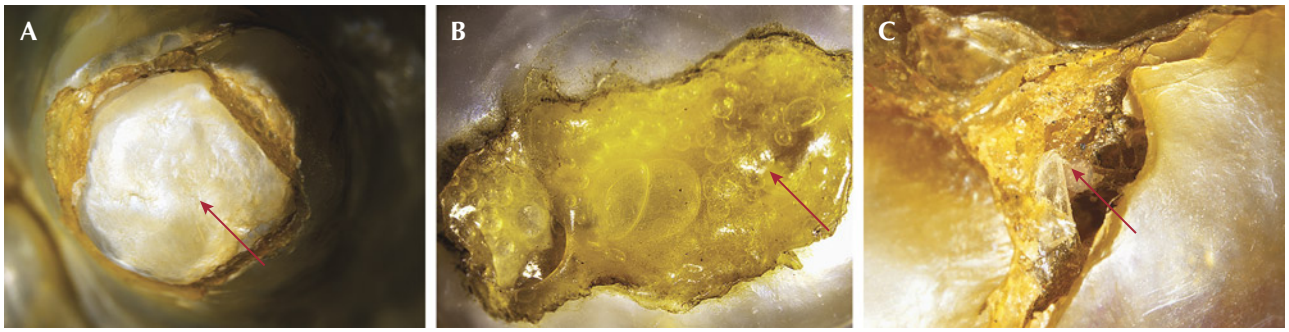

Figure 16. A: Plugged area showing shell piece in the 34.30 ct pearl. B: Trapped gas bubbles in adhesive in the 75.86 ct pearl. C: Adhesive-filled cracks and broken nacre in the 98.53 ct pearl. Photomicrographs by Nitin Wadgaonkar; fields of view 3.00 mm.

reaction could potentially be attributed to the unidentified material inside these filled natural hollow pearls. Under long-wave UV, the pearls showed a moderate bluish reaction, and an inert reaction under short-wave UV radiation.

All four pearls displayed evidence of considerable efforts to improve their durability, including cavity filling, plugging, and working their surfaces to smooth the areas around the plugs. However, despite these interventions, the overall shape, external appearance, and internal structures of the pearls indicate their natural origin. The unique shape and modifications applied to certain areas raise a degree of uncertainty regarding whether they are whole or blister pearls. Nevertheless, their distinctive heart shapes, along with their striking red fluorescence, make these pearls particularly noteworthy.

Eram Shaikh, Nishka Vaz, and Abeer Al-Alawi

Figure 17. Top: RTX images showing the complex internal structure of the four natural hollow pearls filled with unidentified foreign material. Bottom: µ-CT images showing the detailed outline of rectangular and tabular cut fragments used as filler and the pearl openings plugged with shell (indicated with arrows).